GEAP-4383
AEC RESEARCH AND
DEVELOPMENT REPORT
OCTOBER 7, 1963

ACCENT ON VALUE

FUEL CYCLE PROGRAM
A BOILING WATER REACTOR
RESEARCH AND DEVELOPMENT PROGRAM

THIRTEENTH QUARTERLY PROGRESS REPORT
JULY–SEPTEMBER 1963

Compiled By
C.L. HOWARD

U.S. ATOMIC ENERGY COMMISSION
CONTRACT AT(04–3)–189
PROJECT AGREEMENT 11

ATOMIC POWER EQUIPMENT DEPARTMENT
GENERAL ELECTRIC
SAN JOSE, CALIFORNIA

GEAP-4383
AEC Research
and Development Report
October 7, 1963

FUEL CYCLE PROGRAM

A BOILING WATER REACTOR RESEARCH AND DEVELOPMENT PROGRAM

THIRTEENTH QUARTERLY PROGRESS REPORT

July - September 1963

Compiled by
C. L. Howard

U. S. ATOMIC ENERGY COMMISSION
CONTRACT AT(04-3)-189
PROJECT AGREEMENT 11

Printed in U. S. A. ~~Price $1.00.~~ Available from the Office of Technical Services, Department of Commerce, Washington 25, D. C.

ATOMIC POWER EQUIPMENT DEPARTMENT
GENERAL ELECTRIC
SAN JOSE, CALIFORNIA

1443-T10-2

Approved by:

C. L. Howard

C. L. Howard, Project Engineer
Fuel Cycle Development Program

D H Imhoff

D. H. Imhoff, Manager
Engineering Development

ATOMIC POWER EQUIPMENT DEPARTMENT
GENERAL ELECTRIC
SAN JOSE, CALIFORNIA

TABLE OF CONTENTS

LIST OF ILLUSTRATIONS

LIST OF TABLES

INTRODUCTION

The Fuel Cycle Program is an integrated program of investigation in the Vallecitos Boiling Water Reactor (VBWR) and other facilities to improve the technological limits of boiling water reactors in the following areas:

Task A

1. Extend fuel life information on oxide fuel at high specific power operation and raise the performance limits of oxide fuels.
2. Study power stability and performance characteristics of an oxide-fueled core under natural and forced circulation to improve design limits.

Task B

Conduct out-of-pile experiments in heat transfer and fluid dynamics in the areas of burnout heat transfer, steam void observational studies, and two-phase pressure drop to support in-core work.

Task C

Study long-term reactivity and isotopic composition changes for fuels having lattice characteristics of large power reactors.

This report is written in partial fulfillment of contract AT(04-3)-189, Project Agreement No. 11, Fuel Cycle Program, between the United States Atomic Energy Commission and the General Electric Company. Prior reports to the Commission under this contract have included the following:

1. GEAP-3516, First Summary Progress Report, March 1959 - July 1960.
2. GEAP-3558, First Quarterly Progress Report, August - September 1960.
3. GEAP-3627, Second Quarterly Progress Report, October - December 1960.
4. GEAP-3628, Prediction of Two-Phase Flow From Mixing Length Theory, S. Levy, December 27, 1960. Revision I, May 31, 1961.
5. GEAP-3709, Third Quarterly Progress Report, January - March 1961.
6. GEAP-3655, Pressure Drop Along a Fuel Cycle Fuel Assembly, Various Orifice Configurations, E. Janssen and J. A. Kervinen, May 22, 1961.
7. GEAP-3781, Fourth Quarterly Progress Report, April - June 1961.
8. GEAP-3794, Plan for VBWR Stability Experiment, W. H. Cook, et al, August 30, 1961.
9. GEAP-3835, Fifth Quarterly Progress Report, July - September 1961.
10. GEAP-3898, Sixth Quarterly Progress Report, October - December 1961.
11. GEAP-3953, Seventh Quarterly Progress Report, January - March 1962.
12. GEAP-3766, Critical Heat Flux and Flow Pattern Characteristics of High Pressure Boiling Water in Forced Convection, F. E. Tippets, April 1962.

13. GEAP-3961, Prediction of the Critical Heat Flux in Forced Convection Flow, S. Levy, June 20, 1962.

14. GEAP-4048, Eighth Quarterly Progress Report, April - June 1962.

15. GEAP-4061, Water Surface Waves in Boiling Water Reactors, C. L. Howard and R. G. Hamilton, August 31, 1962.

16. GEAP-4094, Ninth Quarterly Progress Report, July - September 1962.

17. GEAP-4098, Evaluation of Zirconium 1.5 W/O Niobium Cladding for Use in Boiling Water Environments, C. J. Baroch and W. C. Rous, October 1962.

18. GEAP-4107, Heavy Element Isotopic Analysis of UO_2 Fuel Irradiated in the VBWR, Report No. 1, M. R. Hackney and C. P. Ruiz, December 1962.

19. GEAP-4159, Tenth Quarterly Progress Report, October - December 1962.

20. GEAP-3899, Burnout Conditions for Single Rod in Annular Geometry, Water at 600 to 1400 psia, E. Janssen and J. A. Kervinen, February 1963.

21. GEAP-4203, Methods for Improving the Critical Heat Flux of BWR's, C. L. Howard, March 1963.

22. GEAP-3653, AEC Fuel Cycle Program, Design and Fabrication of the Basic Fuel Assemblies, C. J. Baroch, J. P. Hoffman and W. C. Rous, March 1963.

23. GEAP-4206, Evaluation of the Failed BMI Hot Gas Isostatic Pressed Fuel Rods, C. J. Baroch, C. B. Boyer and S. W. Porembka, March 1963.

24. GEAP-4215, Eleventh Quarterly Progress Report, January - March, 1963.

25. GEAP-4257, Design and Fabrication of Fuel Rods Containing Low Temperature Sintered Pellets, C. J. Baroch, May 15, 1963.

26. GEAP-4282, Design and Fabrication of Coextruded Stainless Steel Clad - UO_2 Fuel Rods, C. J. Baroch, June, 1963.

27. GEAP-3755, Burnout Conditions for Nonuniformly Heated Rod in Annular Geometry, Water at 1000 psia, E. Janssen and J. A. Kervinen, June, 1963.

28. GEAP-4301, Twelfth Quarterly Progress Report, July - September, 1963.

29. GEAP-4312, Design and Fabrication of Special Assembly 12-L, Two Designs for Utilizing Boron as Burnable Poison, S. Y. Ogawa and H. E. Williamson, July 15, 1963.

30. GEAP-4394, Design and Fabrication of Special Assembly 10L, Compacted Powder Fuel Rods Clad with 0.127 mm Wall Stainless Steel, S. Y. Ogawa and H. E. Williamson, September, 1963.

31. GEAP-4358, Critical Heat Flux for Multirod Geometry, J. E. Hench, September, 1963.

SUMMARY

Task A - Advanced Fuel Power - Limit Tests

1. Fuel irradiations in the VBWR have resulted in exposure increases of 1000 MWD/T (average) for the lead assemblies of each type. The September, 1963 exposure status is as follows:

Fuel Designation and Clad	Number of Assemblies Under Test	Burnup, MWD/T	
		Average of Group	Average for Lead Assembly
H - Annealed stainless (Control rod follower)	10	6800	8265
I - Cold worked stainless	14	6230	8086
J - Zircaloy	23	5570	8445
L - Special	11	--	6526

2. The fuel continues to operate satisfactorily. Fuel assemblies 14 J and 9 H have small fission gas leakages, but no visible cracks or defects.

3. Topical reports describing two of the special fuel assemblies have been prepared. They are titled Design and Fabrication of Special Assembly 12-L, Two Designs for Utilizing Boron as a Burnable Poison and Design and Fabrication of Special Assembly 10-L, Compacted Powder Fuel Rods Clad with 0.127 mm Wall Stainless Steel. Summaries of these reports are presented.

4. Physical property tests on irradiated 304 stainless steel, Zircaloy-2 and Zircaloy-4 fuel cladding have been made. This preliminary data indicates the trend in hardening of the materials as a function of fast flux exposure.

5. The residual stresses of non-irradiated stainless steel clad material have been measured. The surface tensile hoop stress was variable from 43 to 2660 kg/cm^2 (610 to 37,800 lb/in^2) for different samples.

6. The residual hoop stresses in stainless steel tubing were correlated to the time to failure in boiling magnesium chloride (chloride stress corrosion). The relative lifetimes of HPD and Fuel Cycle clad in boiling $Mg\ Cl_2$ do not agree with their relative lifetimes in the reactor.

7. Fabrication of Incoloy-clad fuel assemblies 2L and 3L was completed. Irradiation of 3L began in July and 2L is to begin in October.

8. Stability loop data for the velocity response to a sinusoidal variation in power input are presented. The experimental and calculated results are similar in character and in frequency of the resonance response. A strong sensitivity to subcooling is shown for calculations made for the same exit quality.

Task B - Heat Transfer and Fluid Dynamics

1. A terminal topical report Critical Heat Flux for Multirod Geometry has been issued. The four-rod geometry results in a somewhat higher critical heat flux than for a single rod.

2. Tabulated data for critical heat flux in annular geometry with a "rough liner" is given to complete the reporting of the heat transfer work.

TASK A - ADVANCED FUEL POWER-LIMIT TESTS

A. Irradiation in VBWR

This task provides for irradiation of the special and basic fuel assemblies in VBWR. Summaries of the operating and core loading schedules for the next three months are shown in Tables I and II. The increments of fuel exposure achieved this quarter are shown in Tables III and VI. The lead assemblies of each type gained approximately 1000 MWD/T.

B. Basic Fuel Program

The basic fuel program includes the irradiation and examination of a large number of stainless steel and Zircaloy clad fuel assemblies operated at high specific power to long life in a boiling water reactor. A brief description and the current status of the 50 assemblies are listed in Table III and summarized below.

Designation and Clad	Number	Burnup, fission/cc (MWD/T)(1) Average of Group	Average of Lead Assembly(2)
H - Annealed stainless (Control rod follower)	10	1.86×10^{20} (6800)	2.26×10^{20} (8265)
I - Cold worked stainless(3)	14	1.71×10^{20} (6230)	2.21×10^{20} (8086)
J - Zircaloy(3)	23	1.52×10^{20} (5570)	2.31×10^{20} (8445)

(1) Burnup as of run number 161 which was completed on September 1, 1963.
(2) Peak exposure is about 1.65 times this value.
(3) Average does not include assemblies whose irradiation has been terminated.

The Basic Fuel assemblies continue to operate satisfactorily. On occasion, the in-core sampler and sipping both in the VBWR and in the VBWR pool have indicated that assemblies 9H and 14J may contain defective fuel rods. The data, however, from the in-core sampler and sipping have been inconclusive. Furthermore, visual examination of the assemblies in the VBWR pool has not revealed any defects. Consequently, the irradiation of the assemblies is continuing.

Fuel Sipping and Inspection

Assemblies 9I, 4J, 13J, 14J, and 25J were sipped in the reactor vessel following VBWR run 160. The results of the sipping indicated that the only assembly which may have contained a defective fuel rod was 14J. During VBWR run 161, assembly 14J was placed under the in-core sampler. The in-core sampler indicated that this assembly might contain a defective fuel rod.

Following VBWR run 161, assemblies 5H, 6H, 7H, 9H, 10H, 8I and 14J were sipped in the VBWR pool. Only assembly 9H gave an indication of containing a defective fuel rod. However, visual examination of 9H in the VBWR pool did not reveal any failures; consequently, 9H was returned to the core for run 162.

TABLE I

VBWR OPERATION SCHEDULE

September 1 - September 13	Shutdown. Control rod replacement.
September 15 - October 6	Power operation.
October 6 - October 16	Shutdown. Control rod blocks and Change ESADE Fuel
October 16 - November 17	Power operation.
November 17 - November 24	Shutdown.
November 24 - December 14	Power operation.
December 15 - December 18	Shutdown. Refueling if necessary.
December 19 - January 19	Power operation.
January 20 - January 27	Shutdown, change ESADE fuel.

TABLE II

VBWR CORE COMPOSITION

	Fuel Elements in Core on			
	September 30	October 31	November 30	December 31
Fuel Cycle				
A-2 Basic	10	8	8	8
A-2 Special	10	11	11	11
A-1 Driver	38	38	38	38
	58	57	57	57
Consumers HPD	9	11	10	10
Plutonium	1	1	1	1
Dresden	1	1	1	1
Savannah I	3	3	3	3
Savannah II	5	5	5	5
General Development	2	1	2	2
ESADE	4	4	4	4
Test Assemblies	83	83	83	83
APED Drivers				
Rod	20	15	15	14
Plate	11	11	12	13
Total Fuel	115	110	110	110

TABLE III

CURRENT STATUS OF BASIC FUEL ASSEMBLIES

Group	Assembly Number	Clad* Material	Thickness of Clad cm	Enrichment percent	Target Peak Specific Power kw/kg	Target Peak Heat Flux Watts/cm^2 (Btu/hr-ft^2)	Total Exposure Fissions/cc × 10^{-20} (MWD/T of U)		Exposure Increase This Quarter	
A-2(Reference)										
I	1I	304 Stainless Steel	0.038	3.2	49	154 (488,000)	1.83	(6692)	0.27	(977)
	8I	304 Stainless Steel	0.038	3.2			2.22	(8086)	0.26	(965)
	11J	Zircaloy-2	0.056	3.5			2.31	(8445)	0.20	(771)
	12J	Zircaloy-2	0.056	3.5			2.27	(8292)	0.25	(892)
	13J	Zircaloy-2	0.056	3.5			2.25	(8196)	0.23	(840)
	25J	Zircaloy-2, -4	0.056	4.3			1.24	(4543)	0.25	(892)
II	9I	304 Stainless Steel	0.038	3.2	40	123 (390,000)	2.19	(7990)	0.27	(996)
	16I	304 Stainless Steel	0.038	3.2			1.96	(7148)	0.26	(958)
	9J	Zircaloy-2	0.056	3.2			1.69	(6172)	0.21	(774)
	14J	Zircaloy-2	0.056	3.5			2.09	(7629)	0.26	(930)
III (Isotopic)	18J	Zircaloy-2	0.056	2.7	--	---	1.39	(5072)	0.19	(706)
IV (Pu Recycle)	23J	Zircaloy-2	0.056	2.7	--	---	1.01	(3703)	0.14	(522)
Terminated	6I	304 Stainless Steel	0.038	3.2	--	---	1.54	(5630)	---	---
	11J	304 Stainless Steel	0.038	3.2	--	---	1.59	(5810)	---	---
	8J	Zircaloy-2	0.056	3.2	--	---	1.33	(4840)	---	---
A-1(Driver) V	1J	Zircaloy-2	0.056	2.7	20	63 (200,000)	1.40	(5118)	0.13	(482)
	2J						1.14	(4170)	0.11	(407)
	3J						1.14	(4152)	0.10	(376)
	4J						1.45	(5276)	0.12	(448)

(Continued)

*The I assemblies are clad with cold worked (~5,980 kg/cm^2 yield) stainless steel and the type H assemblies are clad with annealed (~2,820 kg/cm^2 yield) stainless steel.

TABLE III - Current Status of Basic Fuel Assemblies (Continued)

Group	Assembly Number	Clad* Material	Thickness of Clad cm	Enrichment percent	Target Peak Specific Power kw/kg	Target Peak Heat Flux Watts/cm^2 (Btu/hr-ft^2)	Total Exposure Fissions/cc × 10^{-20} (MWD/T of U)		Exposure Increase This Quarter	
A-1(Driver) V (Cont.)	5J	Zircaloy-2	0.056	2.7	20	63 (200,000)	1.63	(5954)	0.17	(622)
	6J						2.03	(7402)	0.23	(843)
	7J						1.45	(5280)	0.14	(507)
	17J						1.33	(4839)	0.17	(631)
VI Instrumente	15I	304 Stainless Steel	0.038	3.5	--	---	0.82	(3006)	0.15	(562)
	21J	Zircaloy-2	0.056	3.0	--	---	1.12	(4104)	0.21	(768)
	22J	Zircaloy-2	0.056	3.2	--	---	1.27	(4635)	0.16	(588)
A-1(Drivers) VII	10J	Zircaloy-2	0.056	3.0	20	63 (200,000)	1.36	(4968)	0.16	(583)
	15J			3.0 & 3.5			1.38	(5022)	0.17	(625)
	16J			2.7			1.66	(6069)	0.19	(700)
	19J			2.7 & 3.0			1.28	(4664)	0.21	(774)
	20J			3.0			1.20	(4390)	0.16	(575)
	2I	304 Stainless Steel	0.038	3.2			1.65	(6015)	0.24	(895)
	3I						1.75	(6404)	0.17	(619)
	4I						1.85	(6771)	0.25	(917)
	5I						1.41	(5134)	0.10	(880)
	7I						1.51	(5517)	0.13	(478)
	10I						1.63	(5943)	0.14	(500)
	12I						1.63	(5949)	0.19	(694)
	13I						1.75	(6387)	0.22	(820)
	14I						1.72	(6264)	0.16	(572)
VIII Control Rod Followers	1H	304 Stainless Steel	0.051	2.7	20	63 (200,000)	1.51	(5529)	0.17	(622)
	2H						1.51	(5525)	0.14	(497)
	3H						1.75	(6360)	0.17	(638)
	4H						2.17	(7925)	0.24	(866)
	5H						1.95	(7100)	0.22	(810)

(Continued)

*The I assemblies are clad with cold worked (~5,980 kg/cm^2 yield) stainless steel and the type H assemblies are clad with annealed (~2,820 kg/cm^2 yield) stainless steel.

TABLE III - Current Status of Basic Fuel Assemblies (Continued)

Group	Assembly Number	Clad* Material	Thickness of Clad cm	Enrichment percent	Target Peak Specific Power kw/kg	Target Peak Heat Flux Watts/cm^2 (Btu/hr-ft^2)	Total Exposure Fissions/cc × 10^{-20} (MWD/T of U)		Exposure Increase This Quarter	
VIII Control Rod Followers (Cont.)	6H	304 Stainless Steel	0.051	2.7	20	63 (200,000)	1.79	(6545)	0.21	(769)
	7H	↓	↓	↓	↓	↓	1.90	(6928)	0.20	(713)
	8H						2.04	(7444)	0.24	(882)
	9H						2.26	(8265)	0.22	(813)
	10H						1.84	(6723)	0.17	(616)

*The I assemblies are clad with cold worked (~5,980 kg/cm^2 yield) stainless steel and the type H assemblies are clad with annealed (~2.820 kg/cm^2 yield) stainless steel.

TABLE IV

RESULTS OF TENSILE TEST OF IRRADIATED CLAD

Test Temperature 343 C - Irradiation Temperature 285 C

Rod Number	Material	Integrated Fast Flux >1 mev	Yield Strength† kg/cm²	Ultimate Tensile Strength† kg/cm²	Uniform Elongation percent	Total Elongation percent
	Zircaloy					
Control	Zircaloy-4	0	1840	2590	2.1	7.9
R8H5	25J Clad	2.1×10^{20}	2580	3250	1.0	3.8
Control	Zircaloy-2	0	1740	2420	3.9	7.8
R5H19	25J Clad	9×10^{19}	2040	2610	2.7	9.0
R2D88	12J Clad	1.4×10^{20}	2370	3010	1.4	4.3
R5H19	25J Clad	2.1×10^{20}	2920	3230	0.7	4.6
R2D88	12J Clad	4.3×10^{20}	2790	4140	1.1	2.0
	304 S.S.					
Control	Type I Clad	0	4550	5790	2.7	4.5
202-F	1I Clad	4.6×10^{20}	5820	6540	2.1	5.8
202-F	1I Clad	4.6×10^{20}	7140	7480	0.65	4.2
Control	304 S.S.	0	4220	4740	3.3	7.8
4.3-4	1L Clad	2.8×10^{20}	6870	7040	0.7	4.0

†To convert kg/cm² to lb/in.², multiply by 14.2.

During the outage following run 161, assemblies 5H, 6H, 7H, 9H, and 10H were inspected in the VBWR pool. Other than for handling scratches and one broken spacer wire, the assemblies were in excellent condition. There was no indication of excessive crud deposition and no indications of crud spalling.

Tensile Properties

The 343 C (650 F) tensile properties of the irradiated clad from the I, J, and L assemblies were determined. The results of the tests are presented in Table IV. The low values for total elongation are believed to be associated with the specimen configuration, rather than a loss of ductility. However, the values for uniform elongation are consistent with those reported in the literature and therefore appear to be unaffected by specimen configuration.

The Zircaloy data are in agreement with most of the data which has been reported by other investigators[1] in that:

1. Both the tensile and yield strengths increase with increasing fast neutron exposure. However, the yield strength increases at a faster rate than the tensile strength.
2. The uniform elongation diminishes quite rapidly, and after fast flux exposures of 3 to 5×10^{20} nvt (.1 mev) the uniform elongation is less than 1 percent.

Some of the tensile data reported by other investigators indicates that both the tensile and yield strength saturate; i. e., there is no further increase in tensile or yield strength with increasing irradiation. The Fuel Cycle data covers too narrow a band to determine whether saturation has been achieved. The data which was obtained, however, falls on a relatively straight line as shown in Figure 1.

The magnitude of the change in tensile strength does not agree with the data reported in WAPD-TM-326[2] as shown in Figure 2. Using the same definition of fast flux as the WAPD report would shift the Fuel Cycle data to the right, but would not change the slope of the line. The differences in irradiation and tensile test temperature may explain the difference in slope. The data reported in the WAPD report also do not show signs of saturation even after exposures of 10^{22} nvt

There is very little data available with which to compare the stainless steel tensile data, primarily because of the difference in test and irradiation temperatures. The unusually low uniform elongations reported in Table IV are believed to be associated with the specimen configuration rather than with a gross loss in ductility. Similarly low elongations were observed in irradiated clad from the High Power Density Program[3]. However, burst tests of the HPD tubing indicate that the cladding has much greater ductility than indicated by the tensile tests[4].

The tensile and yield strengths versus neutron exposure are plotted in Figure 3. As with the Zircaloy-2, there are no signs of saturation, but again the exposures are too low to draw firm conclusions.

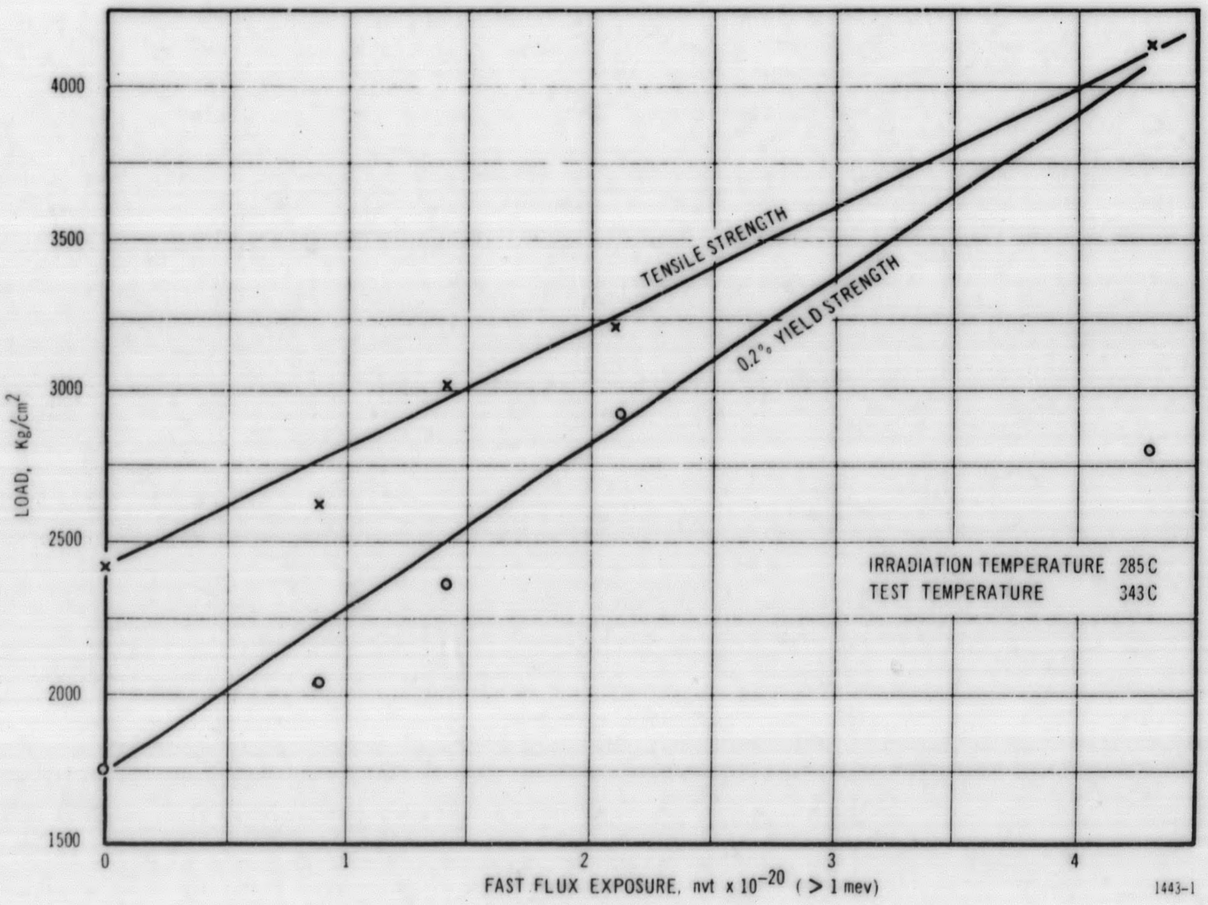

Figure 1. Effect of Irradiation on the Properties of Zircaloy-2

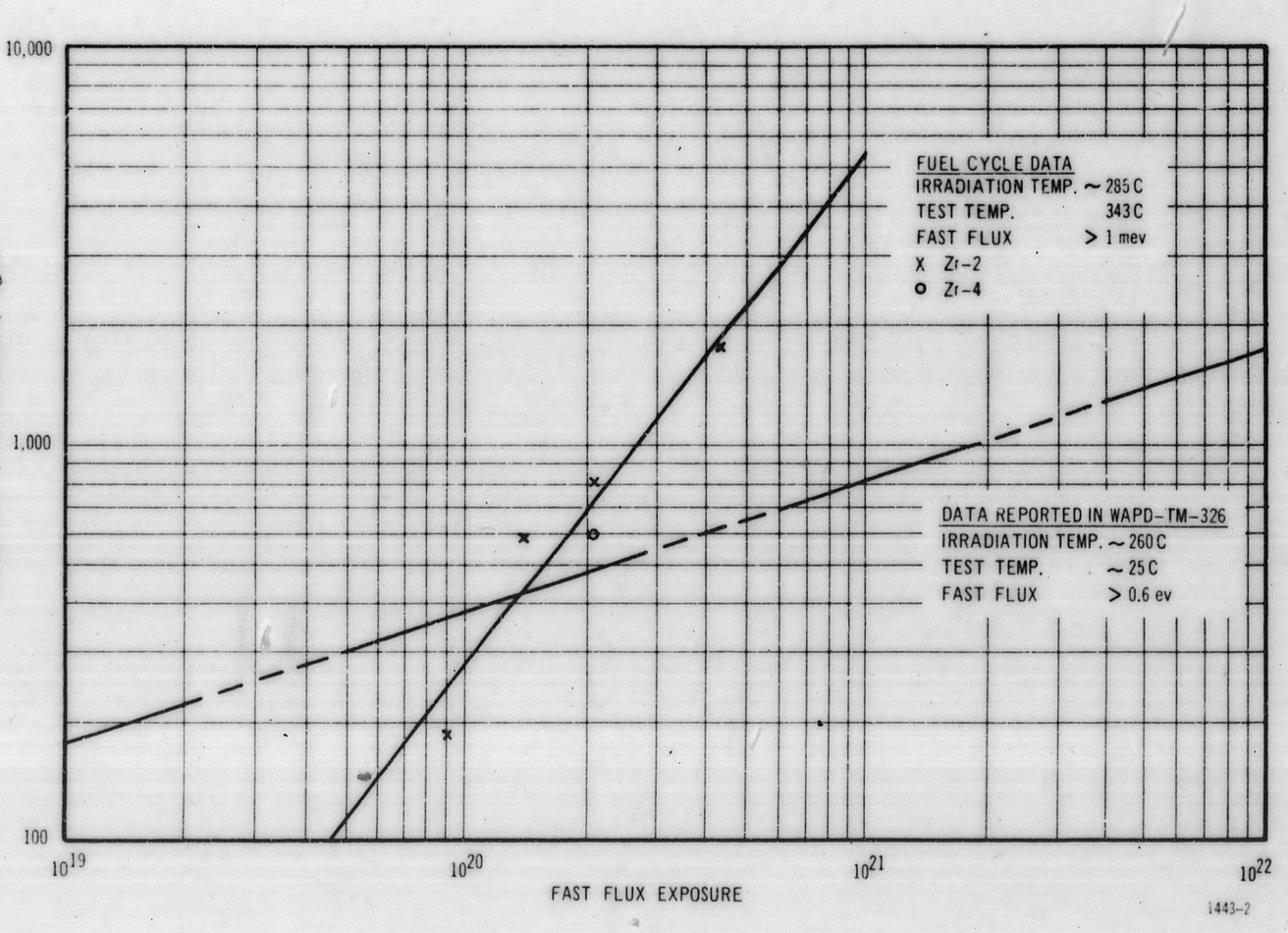

Figure 2. Change in Tensile Strength of Zircaloy-2 as a Function of Fast Flux Exposure

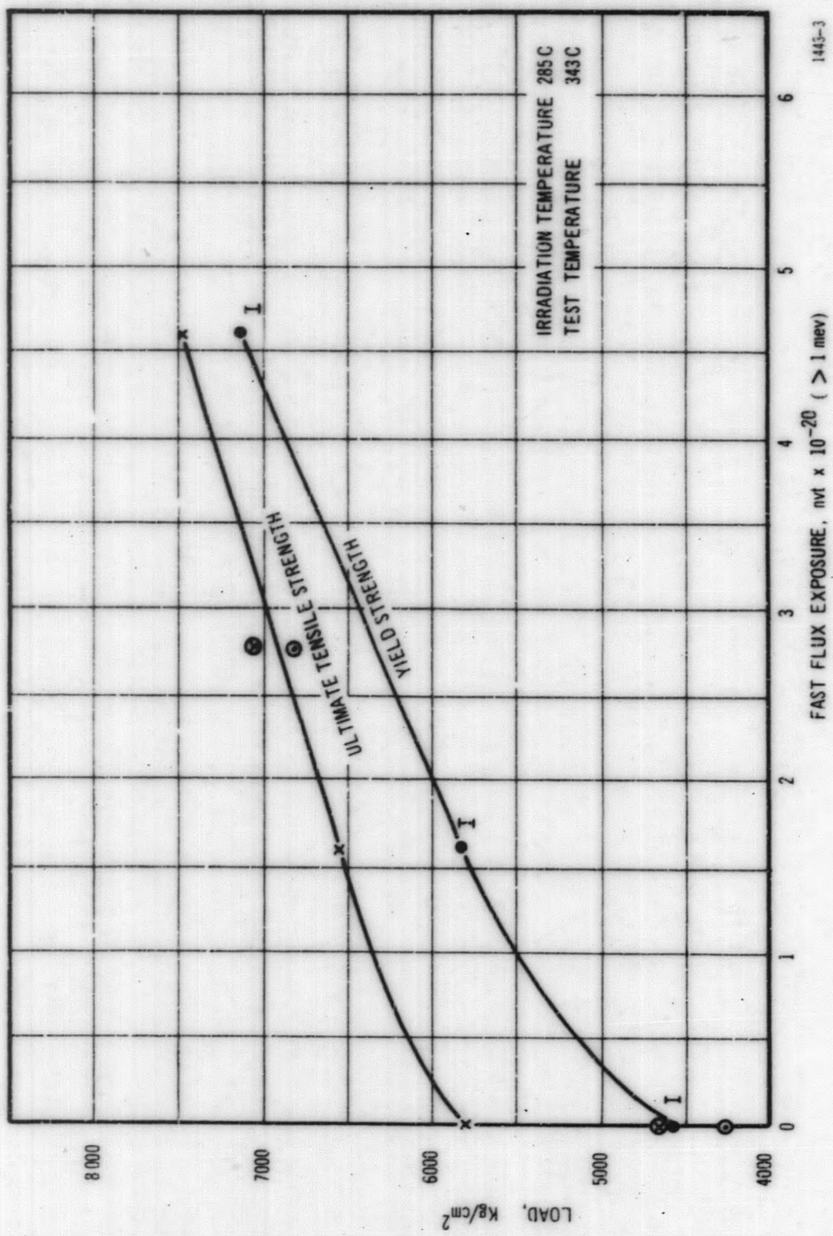

Figure 3. Effect of Irradiation on the Tensile Properties of 304 Stainless Steel

Residual Stresses in Stainless Steel Cladding

The evaluation of the fuel rod failures observed in the High Power Density Program indicate that the sum of the stresses in the clad significantly influence the time to failure. Residual stresses in the stainless steel cladding resulting from the various fabrication operations were determined to aid in the evaluation of the Fuel Cycle cladding with respect to the HPD cladding.

The formulas developed by Sachs and Espey[5] for residual stress in thin-walled tubing have been applied to clad sections cut from fuel rods, which are representative of those being irradiated in VBWR under the Fuel Cycle Program.

Circumferential residual stresses are determined by measuring a diameter change that takes place in a clad sample when the sample is split longitudinally. This can be a direct measurement or can be a measurement derived from a circumference change. The change in circumference is determined by making the longitudinal cut between two hardness impressions on the clad surface. The distance between the impressions is measured before and after splitting the sample. The change in chordal distance is converted to a change in circumferential distance and then the diameter change is calculated from the relation:

$$\Delta D = \frac{\Delta C}{\pi}$$

The residual stress can then be determined from the formula:

$$S_{(max)} = \frac{E}{1 - \nu^2} \; d \; \frac{\Delta D_1}{Dm^2}$$

where:

- $S_{(max)}$ - stress in outer fibers, in psi
- E - modulus of elasticity, in psi
- d - wall thickness, in inches
- ν - Poisson's ratio
- ΔD - Change in diameter, in inches, after splitting
- Dm - Mean diameter, in inches, before and after splitting

The longitudinal residual stresses are determined by slitting a tongue (longitudinal) from specimens split longitudinally to release the circumferential stresses. This causes the strip to deflect in the form of a circular arc. The deflection is measured and the longitudinal stress in the outside fiber is calculated using the equation:

$$S = Edf/L^2$$

where:

- S - longitudinal stress in the outside fiber, in psi
- E - Modulus of elasticity, in psi
- d - Original wall thickness, in inches
- f - total deflection, in inches, of the tongue
- L - length, in inches, of the tongue

The surface stresses in the as-received tubing from various clad types are presented in Table V; positive values indicate tensile stresses. An effort was made to determine whether the differences in residual stresses were real and to determine whether there are any gross differences between the HPD and Fuel Cycle clad materials. One of the easiest methods of detecting the differences is the $MgCl_2$ test using a boiling solution containing 42 w/o $MgCl_2$. This test is not construed to represent actual performance capabilities of the materials. However, this test may serve to evaluate the relative resistance of various materials to a stress-sensitive type of failure which is believed to have occurred with 304 stainless steel in nuclear environments. The results of the $MgCl_2$ test are also included in Table V.

A plot of time to failure in boiling $MgCl_2$ versus residual circumferential (hoop) stresses is shown in Figure 4. Plotting time to failure versus circumferential stresses rather than longitudinal stresses is valid as all tubing except 10L-C1-CW contained longitudinal cracking. This indicated that the hoop stresses were the most important factor causing the cracking. The Fuel Cycle data is compared with the results obtained from the HPD program.[6]

The results presented in Figure 4 indicate that there is considerable difference between the Fuel Cycle and HPD clad materials with regard to susceptibility to transgranular type cracking in boiling $MgCl_2$. There is apparently no correlation with in-reactor performance and the $MgCl_2$ test in that the material which failed first in the $MgCl_2$ has not yet failed in reactor service. The HPD assemblies, similar in design to the "I" assemblies, have failed by intergranular cracking at a group average exposure of 2.07×10^{20} fissions/cc (7540 MWD/T). The "I" assemblies have achieved a group average exposure of 1.71×10^{20} fissions/cc (6230 MWD/T) without failure. The average exposure of the lead "I" assembly has reached 2.22×10^{20} fissions/cc (8086 MWD/T).

The data in Table V and Figure 4 also indicate that the time to failure of cold worked stainless steel is considerably less than that of annealed stainless steel having the same residual stress. This is in close agreement with the classical theory of chloride stress corrosion.

C. Special Fuel Program

The Special Fuel Program includes the irradiation and examination of 11 fuel assemblies based on fuel concepts which show potential for improved fuel cycle economy through increased performance or lower fabricating costs. These assemblies will be operated at high specific power to long life to determine performance capabilities in relation to the basic fuel assemblies which represent current fuel design and fabrication processes.

The Special Fuel Assemblies are divided into the following four groups:

1. Higher Thermal Performance

Operation of fuel at higher thermal performance improves the economics of the fuel cycle, provided that a reasonable fuel lifetime is achieved. Assembly 1L is a test of UO_2 fuel at higher temperatures while assembly 9L provides an evaluation of thermal conductivity improvers.

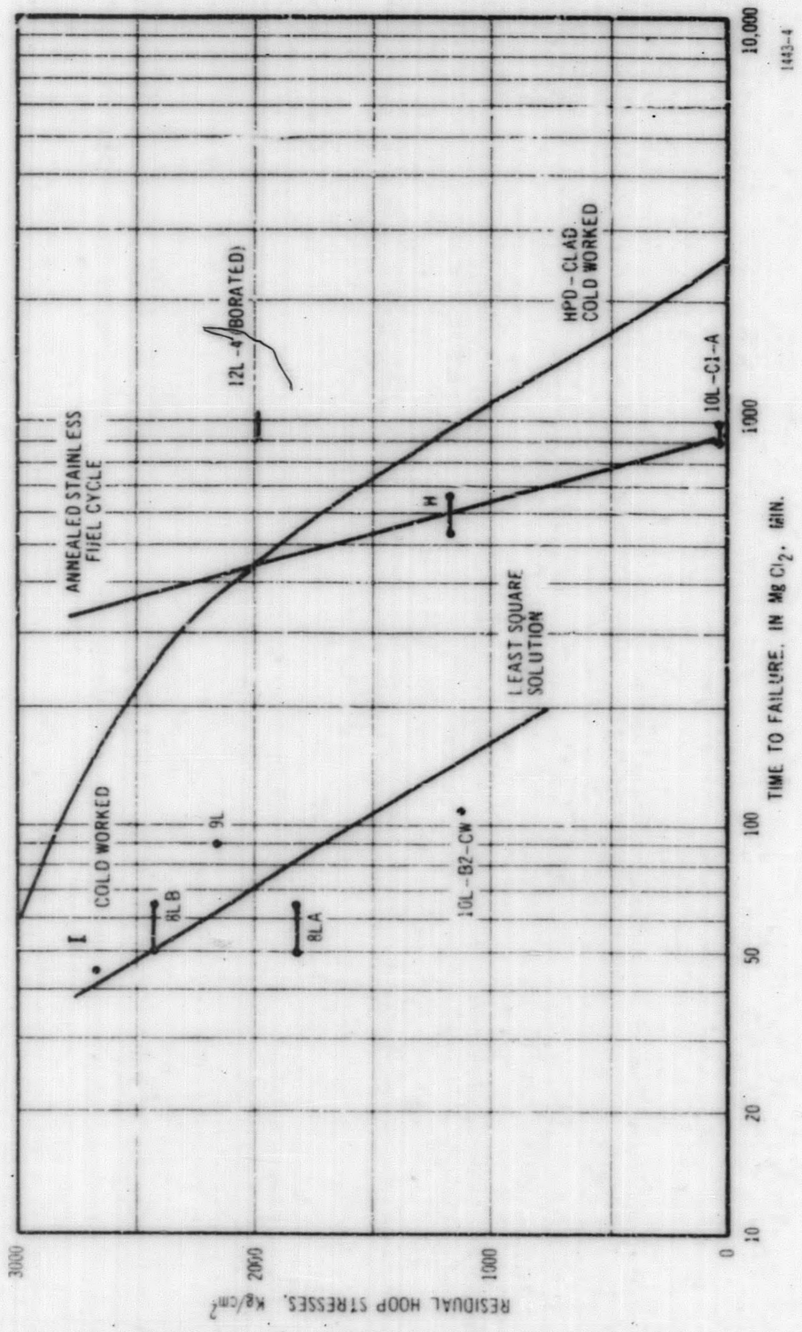

Figure 4. Time to Failure in Boiling Mg Cl_2 Versus Residual Hoop Stress

TABLE V

MAXIMUM RESIDUAL HOOP AND
LONGITUDINAL STRESS IN OUTER FIBERS OF STAINLESS STEEL

Material	Hoop‡ kg/cm^2	Longitudinal‡ kg/cm^2	Time to Failure in Boiling $MgCl_2$ Solution minutes	Nature of Cracking*
H	1170	---	540 - 660	Long
I	2660	---	45	Long
1L	1350	506	160**	---
8LA	1820	1180	50 - 65	Long
8LB	2420	1210	50 - 65	Long
9L	2160	696	90	Long
10L-C1-A	43	1100	900 - 960	Long & Circ
10L-C1-CW	950	1435	90	Circ
10L-B2-CW	1130	2070	120	Long & Circ
12L	892	690	1400**	---
12L-1	328	598 - 1080	1400**	---
12L-4	1990	1025	900 - 1050	Long

*Long - Longitudinal crack; Circ - Circumferential cracking

**Specimens did not crack, test terminated, 1L specimen pitted rather severely, but there was no evidence of cracking.

‡To convert kg/cm^2 to lb/in.^{2}, multiply by 14.2.

2. Alternate Clad Materials

Zirconium alloys provide a low neutron capture cross section fuel clad material which has good corrosion resistance to water at temperatures normally encountered in water-cooled reactors. These alloys are susceptible to hydride embrittlement as a result of corrosion. The hydride problem may be extremely serious if water enters the fuel rod.

The austenitic stainless steels have good corrosion resistance even on the inside surface of defective fuel rods. However, the cross section of the austenitic stainless steels is about 30 times that of Zircaloy-2. Furthermore, beginning in May, 1962, the High Power Density Program has indicated that the stainless steels are susceptible to intergranular attack.

To determine whether the performance and/or fuel cycle costs using stainless steel and Zircaloy clads can be improved, the testing of fuel rods of the following concepts is in progress:

Provide protection to the inside surface of Zircaloy-2 tubing - Assembly 7L.

Improve the hydride resistance of zirconium alloys - Assembly 6L.

Reduce the thickness of the stainless steel clad to a thin shell - Assemblies 8L and 10L.

Improve the resistance of the stainless steels to intergranular attack - Assemblies 2L and 3L.

3. Reduced Fabrication Cost Concepts

Irradiation of assemblies containing fuel rods made by new fabrication processes, which offer potential increases in UO_2 density or cost reductions in the manufacture of UO_2 fuel elements, will provide engineering proof tests of the feasibility of these new methods. The testing of fuel rods fabricated by the following methods is in progress:

a. Low temperature sintered pellets - Assembly 5L.

b. Co-extruded UO_2 and stainless steel clad - Assembly 5L.

c. UO_2 extrusions - Assembly 11L.

4. Extended Life Concepts

The loss of reactivity as the result of fuel burnup may limit the life of the fuel. Initial reactivity for burnup is limited by the capacity of the control system to make the cold, clean core subcritical. The reactivity change associated with the fuel burnup can be reduced by burnable poisons. Assembly 12L is designed to evaluate boron as a burnable poison by: (1) alloying boron with the stainless steel cladding, and (2) mixing a boron compound with the UO_2.

The current status of the 11 Special Assemblies is listed in Table VI. The evaluation of the performance of the 11 assemblies during this quarter was primarily limited to VBWR irradiations and occasional visual inspection and sipping of selected assemblies. All of the special assemblies continue to operate satisfactorily. Sipping following VBWR runs 160 and 161 indicated that Assemblies 5L, 7L, 8L, 10L, and 12L were free of defective fuel rods.

The tubing for assembly 2L was received and the fabrication of the fuel rods was completed. The assembly is scheduled for insertion in the VBWR for run 163 which is scheduled to begin in October, 1963.

The irradiation of Assembly 3L began with VBWR run 161. The VBWR license requires that a new assembly be irradiated in a core location where the peak heat flux is < 88.8 watts/cm^2 (250,000 Btu/hr-ft^2) and then visually inspected before the assembly can be irradiated at a higher heat flux. Following run 161, Assembly 3L was found to be in excellent condition, and, therefore, the assembly was transferred to a core location where the peak heat flux is ~ 126 watts/cm^2 (400,000 Btu/hr-ft^2).

During this quarter GEAP-4312, "Design and Fabrication of Special Assembly 12L, Two Designs for Utilizing Boron as Burnable Poison," by S. Y. Ogawa and H. E. Williamson, July, 1963, was issued. The summary of the report is as follows:

Two reactor fuel rod designs using boron burnable poison have been incorporated into a fuel bundle for irradiation testing in the VBWR. The experiment will provide irradiation experience for these two designs, under actual operation in a boiling water power reactor.

The designs utilize borated stainless steel cladding and a boron compound mixed in compacted powder UO_2 fuel. The test assembly was fabricated for the AEC Fuel Cycle Program and is designated as Special Assembly 12L. Irradiation testing in the VBWR started in February, 1963.

The bundle contains 16 fuel rods in a 4×4 array and is designed to be operated at a peak heat flux of 400,000 Btu/ft^2-hr. The rods have a nominal outside diameter of 0.485 inch; the cladding is 0.011-inch thick Type 304 stainless steel tubing.

The following is a brief summary of the design and fabrication characteristics of the fuel rods in the bundle.

Borated Cladding

The borated stainless steel cladding contains either 500 ppm or 750 ppm natural boron, alloyed with Type 304 stainless steel. Annealed and cold-worked tubing from each boron level were used. Eight rods were fabricated with this type of tubing. Four of these were filled with sintered UO_2 pellets, and the other four with arc-fused powder UO_2, vibratory compacted to 85 percent of theoretical density. The test matrix covers all possible combinations among these three parameters.

TABLE VI

STATUS OF SPECIAL FUEL ASSEMBLIES

Assembly Number	Concept	Clad Material	Rod Diameter cm	Clad Thickness cm	Enrichment percent	Exposure as of 9/1/63 Fissions/cc × 10-20 (MWD/T)	Increase This Quarter Fissions/cc × 10-20 (MWD/T)
1L	Centermelt	304 S. S.	1.308	0.051	4.3	1.59 (5806)	0.24 (869)
2L	Incoloy	Incoloy	1.067	0.051	5.46	fabrication complete	0.00 (0)
3L	Incoloy	Incoloy	1.080	0.025	5.46	0.13 (466)	0.13 (466)
5L	Low temperature sintered pellets	304 S. S.	1.021	0.041	5.5	0.56 (2046)	0.26 (946)
5L	Coextruded UO_2 and stainless steel clad	304 S. S.	1.016	0.038	5.5	1.78 (6526)	0.24 (865)
6L	Zircaloy-4 clad	Zr-2	1.435	0.074	3.9	0.67 (2462)	0.16 (568)
7L	Stainless steel lined Zr-2	Zr-2	1.077	0.0597	4.58	1.55 (5690)	0.0 (0)
8L	0.013-cm stainless steel clad pellets	304 S. S.	0.965	0.013	5.0 & 4.58	1.16 (4245)	0.24 (863)
9L	Thermal conductivity improver	304 S. S.	1.308	0.051	6.5 & 8.0	0.60 (2190)	0.0 (0)
10L	0.013-cm stainless steel clad powder	304 S. S.	0.978	0.013	6.0	0.67 (2480)	0.25 (902)
11L	Extruded UO_2	304 S. S.	1.168 & 1.257	0.051 & 0.056	5.5	0.44 (1620)	0.20 (727)
12L	Burnable poison	304 S. S.	1.232	0.028	5.5 & 6.6	0.58 (2128)	0.25 (930)

The two types of fuels were used for creating different conditions of possible fuel-to-clad mechanical interactions. If the reduction in the clad ductility caused by the transmutation of the boron was acute, the sensitivity of the tubing to such conditions would be increased and the response might be markedly noticeable during the irradiation. The rods containing the pellet fuel had the pellet-to-clad diametral gaps controlled to between 3 to 4 mils. No poison was added to the UO_2 in these rods.

Weld-bead cracking in the joint between the end plug and cladding containing the 750 ppm boron was encountered. The borated stainless steel was susceptible to such cracking because of the hot-short condition due to the boron content. The problem was alleviated by redesigning the end plug and by modifying the welding practice to cause a greater amount of dilution in the weld metal to lower the over-all boron content. It was also important to minimize the heat input during the welding.

Boron in the Fuel

In four other rods, the fuel was poisoned with 50 ppm of natural boron, added as zirconium diboride. This compound was in the form of minus 325-mesh powder for two fuel rods, and in the form of larger sintered particles sized between 100 to 200 microns and coated with a film of molybdenum metal 1 to 3 microns thick for two fuel rods. This coating was used to study its effectiveness as a reaction barrier between the zirconium diboride and the UO_2.

The poison was mixed intimately with the arc-fused UO_2 powder, and the mixture was vibratory loaded and compacted to 85 percent of theoretical density. In each of the rods, the poisoned fuel was bracketed with unadulterated UO_2, as shown in Figure 1-1. Sintered UO_2 disks having the same U^{235} enrichment as the pure UO_2 were used at the interfaces of these two fuel sections to prevent fuel intermixing and boron contamination during the vibratory loading and compaction. The poisoned section was located in the peak flux region of the rods. This fuel arrangement was used to facilitate the positive detection of the occurrence of gross axial boron migration.

Reference Rods

Four reference rods containing no poison whatever were included in the bundle. Three of these were filled with pellet fuel, and one was filled with vibratory-compacted, arc-fused powder fuel.

Adjustments in the fuel enrichments were made among and within the rods to compensate for the different levels of neutron absorption. The rods were thus normalized to operate with the same axial power distribution and at the same power level.

The bundle is scheduled for operation to a design life of 15,000 MWD/T, with cursory visual examinations at convenient interim periods coinciding with scheduled

reactor shutdowns. A gamma-scan monitoring of the power distribution and detailed examination of selected rods are planned after a burnup between 2,000 and 4,000 MWD/T has been achieved. The frequency of further interim detailed examinations will depend upon the performance of the rods with further irradiation, and upon the results of the first detailed examination.

Another topical report, "Design and Fabrication of Special Assembly 10-L, Compacted Powder Fuel Rods Clad with 0.127 mm Wall Stainless Steel," by S. Y. Ogawa and H. E. Williamson has been prepared. The summary is as follows:

Fuel rods clad with 0.1270-mm (0.005-inch) wall stainless steel and filled with vibratory compacted powder UO_2 were fabricated and incorporated into a bundle for irradiation testing in the VBWR. Experience will be gained on the performance capabilities of very thin cladding material by the actual operation of these fuel rods in a boiling water nuclear reactor. The experiment will provide operating data on this cladding material for comparison with those obtained on the same type of material used in fuel rods filled with sintered pellet fuel. This kind of comparison will permit the evaluation of the relative effects of the mechanical interaction between the fuel and the cladding.

The test assembly was fabricated for the AEC Fuel Cycle Program, and is designated as Special Assembly 10-L. There are 16 fuel rods in a 4 by 4 array in the bundle. The rods have a nominal outside diameter of 9.652 mm (0.380 inch), and are designed to be operated at a peak heat flux of 142 watts/cm^2 (450,000 Btu/ft^2-hr). Irradiation of the test assembly was started in February, 1963.

The fuel rod cladding material is type 304 stainless steel tubing. Annealed and cold-worked tubing are being tested.

The compacted bulk UO_2 densities in the rods ranged from 83 to 85 percent of theoretical. Arc-fused and Dyna Pak UO_2 were used. The UO_2 particles manufactured by these two different methods were of high density and had about the same compacting characteristics in this particular usage. Each type of powder is in separate rods.

Differences in the physical characteristics of the fused and Dyna Pak UO_2 were in the microstructures, the particle shapes, and the gas contents. The fused particles were typically equiaxed, whereas the Dyna Pak particles were angular and similar in appearance to crushed flint rock.

The amount of gas released by the fused material was about ten times as much as that released by the Dyna Pak UO_2 at 1700 C (3092 F). Nitrogen, carbon monoxide, and hydrogen were the principal gases evolved by both types of UO_2. The gas evolution tests also revealed that the amounts released at elevated temperatures are related inversely to the particle size tested. The Dyna Pak UO_2 showed an almost linear inverse proportionality.

The measured gas contents were normalized into realistic design release rates in terms of particle sizes and temperature. The total amount of gases to be released by the UO_2 in a fuel rod was calculated with these rates applied to the particle size distribution in the blends used and to the estimated fuel temperatures within the fuel column. The gas plenum was designed to accommodate this additional gas content.

The bundle is planned for operation to reach the maximum exposure of 3.63×10^{20} fissions per cc (15,000 MWD/T). Visual examinations will be performed at convenient interim periods coinciding with scheduled reactor shutdown. Destructive examination of selected rods is planned after a burn-up between 4.92×10^{19} to 9.84×10^{19} fissions per cc (2,000 to 4,000 MWD/T) has been achieved. The frequency of interim detailed examinations will depend upon the performance of the rods with irradiation and upon the results of the first destructive examination.

The performance of the rods in Special Assembly 10-L will be assessed by comparing it with the performance of the rods in Special Assembly 8-L. Assembly 8-L is the VBWR test assembly, also fabricated for the Fuel Cycle Program, which has UO_2 pellet-filled rods clad with the same kind of material.

D. Stability

This task provides for the development of a mathematical stability model to predict the dynamic performance of boiling water reactors, and for stability tests in the VBWR and experiments in a stability loop to provide an experimental basis for the model. The work on this task has been terminated except for completion of terminal reports.

The VBWR test report and noise analysis are still in progress. The final test data from the hydraulic stability loop is reported here as a terminal report on the stability loop work on this program.

Hydraulic Stability Loop

The test loop which is described in GEAP-3935* was operated in natural circulation to examine steady-state, power impulse and power oscillation responses of various parameters, but primarily flow. Steady-state and transient results were reported in GEAP-4215* and 4159.* Some significant understanding of the analytical model was obtained from these runs.

The steady-state responses of flow were shown to be predicted very well by the stability and transient response code. A maximum error of 8 percent in blow at 3 percent steam quality was found. This accuracy of calculation is very good for two-phase flow systems. This conclusion applies to natural circulation operation. No forced circulation tests were conducted under the Fuel Cycle Program.

*Previous reports on this program are listed on page v.

Power impulse tests were conducted to demonstrate the oscillatory characteristics of two-phase flow and to make qualitative observations about the analytical model. The following information was obtained from a power impulse transient test:

1. Damped oscillation frequency.
2. Quadratic damping coefficient.
3. Time lags (or phase) of pressure and velocity to power impulse. Information on pressure propagation.
4. Magnitude and character of pressure and velocity changes.

The following conclusions were reached about two-phase flow transients in channels:

1. Undamped and (self-excited) oscillatory responses are easily obtained by parametric changes and small disturbances.
2. The pressure in the heater rises in response to power oscillations without a change in pressure difference across the channel. The heater fluid acts as a capacitance under these circumstances. This effect seems to be the most energetic effect which presents itself. It seems likely to provide an explanation for some portion of the discrepancies between VBWR test and the theory.
3. Intermediate subcooling operation showed flow responses were less stable than higher or lower subcooling runs.
4. The frequency dependent theory is not, at present, in a form well-suited to prediction of transients.

Power oscillation tests with natural circulation were conducted during May 1963, but not analyzed under Fuel Cycle funding. The data analysis and comparison of experiment and theory are presented here to provide a quantitatively complete representation of the stability and transient response theory. The parametric variation of four runs studied in detail are shown in the following tabulation.

Natural Circulation

SATR Run Number 5-31-01-002	Loop Run Number 5-31-01
V 4.35 fps	4.25 fps
h_s 42.9 Btu/lb	42.7 Btu/lb
X 10.4 percent	11.9 percent
Resistance Type - Minimum	(Flowmeter of unusually high flow resistance)

SATR Run Number 5-24-01-001	Loop Run Number 5-24-01-c
V 4.33 fps	4.24 fps
h_s 14.9 Btu/lb	14.7 Btu/lb
X 7.0 percent	7.1 percent
Resistance Type - Minimum	(Flowmeter of unusually high flow resistance)

SATR Run Number 5-28-01-002	Loop Run Number 5-28-01
V 4.2 fps	4.13 fps
h_s 32.8 Btu/lb	32.8 Btu/lb
X 14.9 percent	14.9 percent
Resistance - Minimum	(Flowmeter of unusually high flow resistance)

SATR Run Number 5-27-01-001	Loop Run Number 5-27-01
V 3.49 fps	3.61 fps
h_s 16.8 Btu/lb	16.8 Btu/lb
X 20.8 percent	21.5 percent
Resistance - Minimum	(Flowmeter of unusually high flow resistance)

The four tests present a preliminary indication of the stability and transient response code results for power oscillation compared to test data. In order to demonstrate the expected variation of velocity responses to subcooling changes, Run Number 5-28-01 is re-calculated for ±40 percent change in subcooling. This gives an evaluation of the change in magnitude of velocity response. Figure 5 shows this sizeable change in velocity response when the exit quality is held constant and inlet subcooling is changed.

Figures 6 through 9 show magnitude and phase plots of the four tabulated runs. These power oscillation runs were briefly discussed in GEAP-4301. The following observations are made on these figures:

1. Magnitude curves of $\frac{V^*}{\gamma^*}$, the velocity response to a power oscillation, follows the amplitude of the harmonics of the flow disturbance surprisingly well, indicating the character of the theoretical response to be correct.
2. Most phase lag curves demonstrate a drift at high frequencies to a greater phase lag than predicted by theory. Some data points exceed 180°, while the theory does not.
3. The high quality (20 percent) intermediate subcooling (16.8 Btu) run 5-27 shows the best correspondence with theory of the four cases.
4. Frequencies of the fundamental appear quite accurately determined in all cases.
5. Lower quality runs appear to produce lower magnitude oscillations and larger phase lags than the theory predicts.
6. Experimentally, it was determined that there was a greater single phase loss than was used in the theoretical calculations. This was due to greater loss in the turbine flowmeter than was expected.

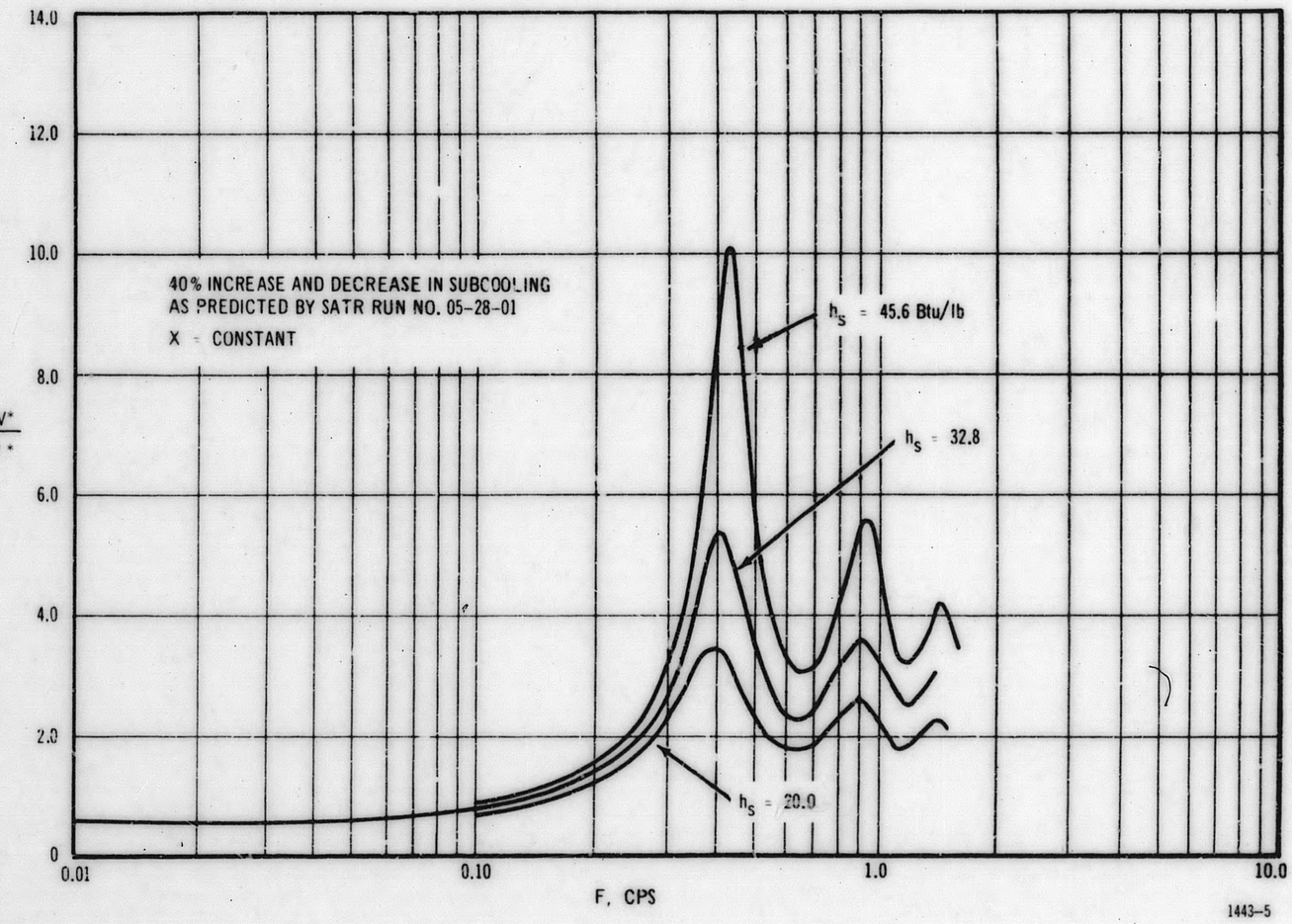

Figure 5. Calculated Effect of Subcooling on Velocity Response

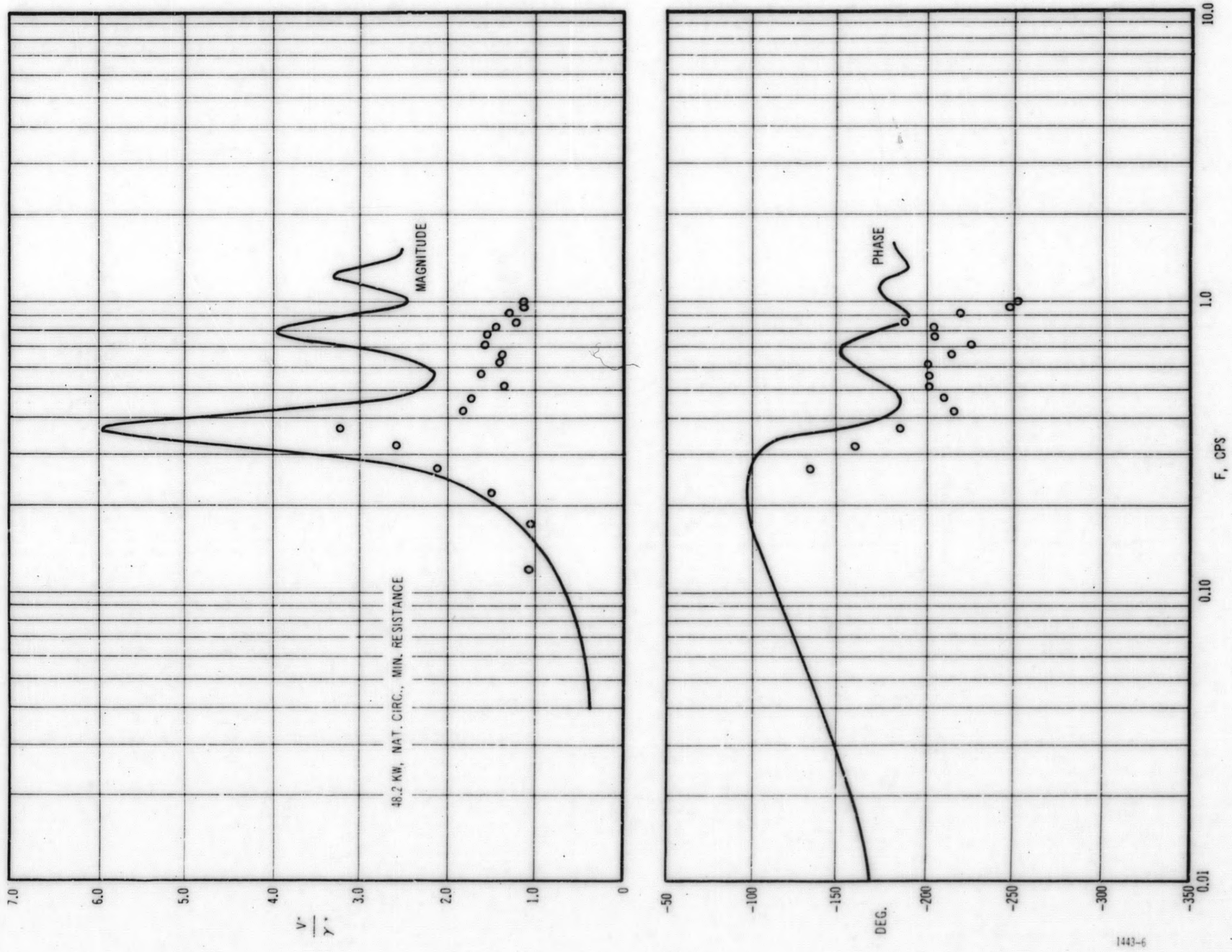

Figure 6. Velocity Response, Run 5-31-01

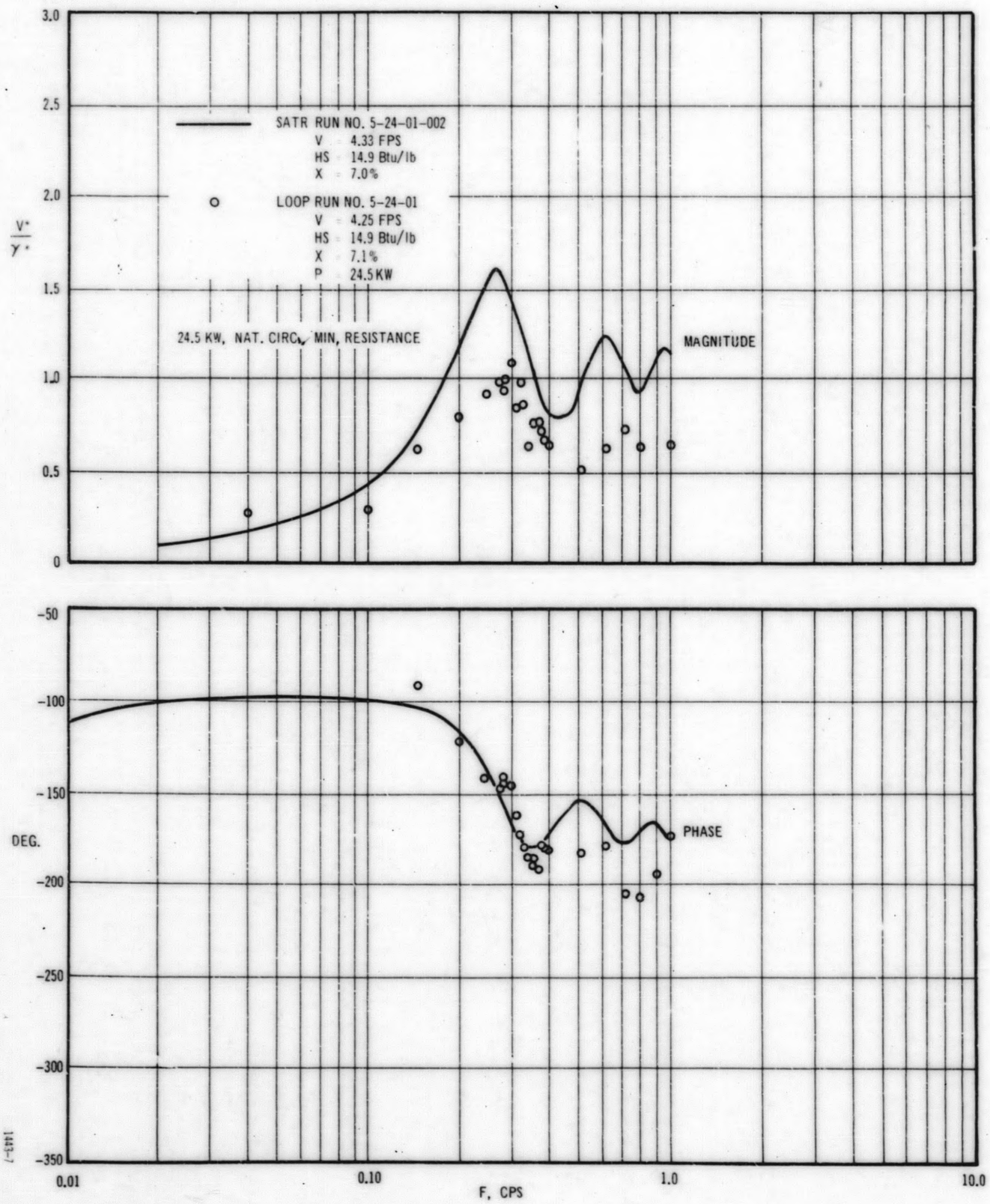

Figure 7. Velocity Response, Run 5-24-01

1443-7

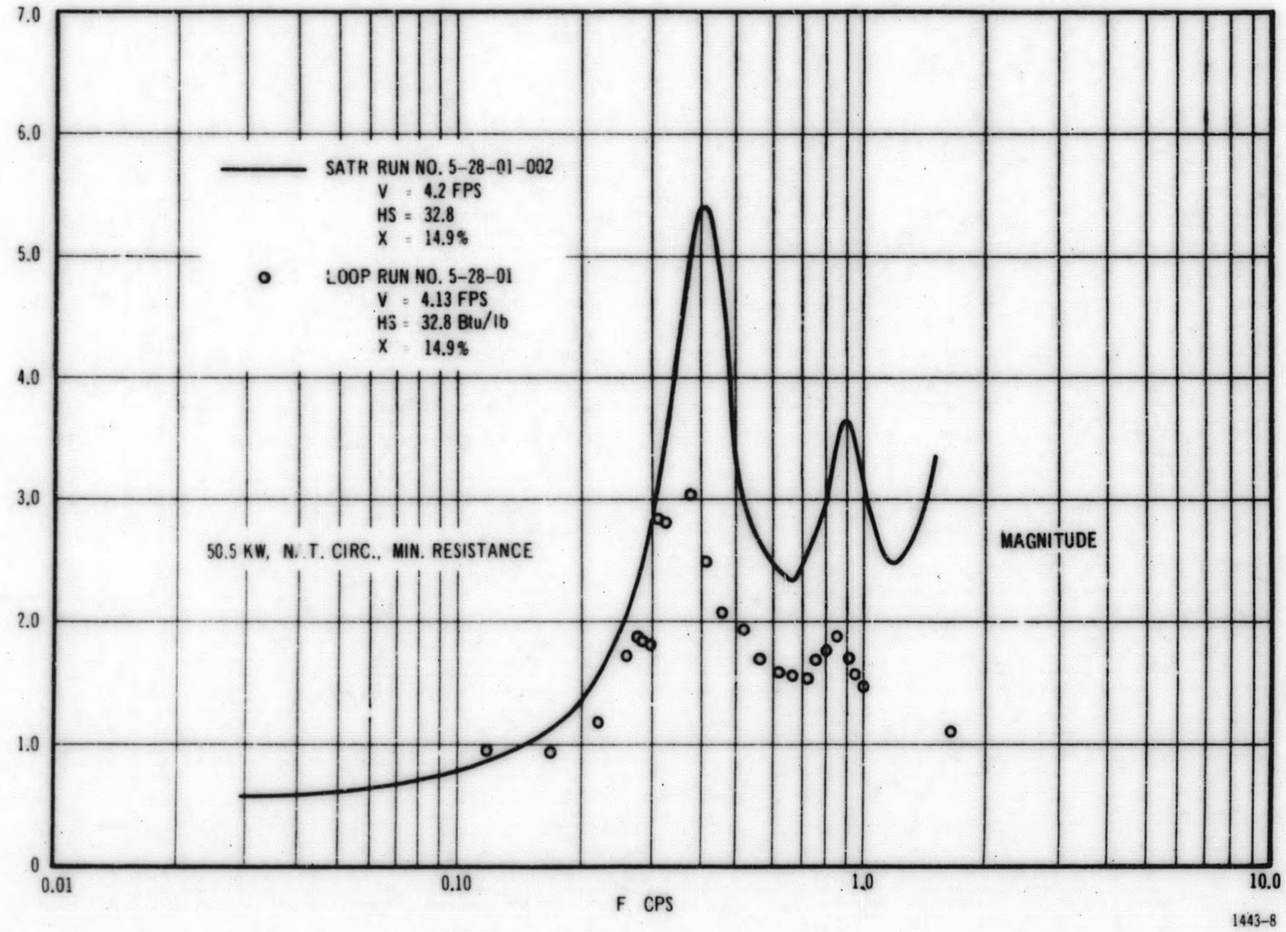

Figure 8. Velocity Response, Run 5-29-01

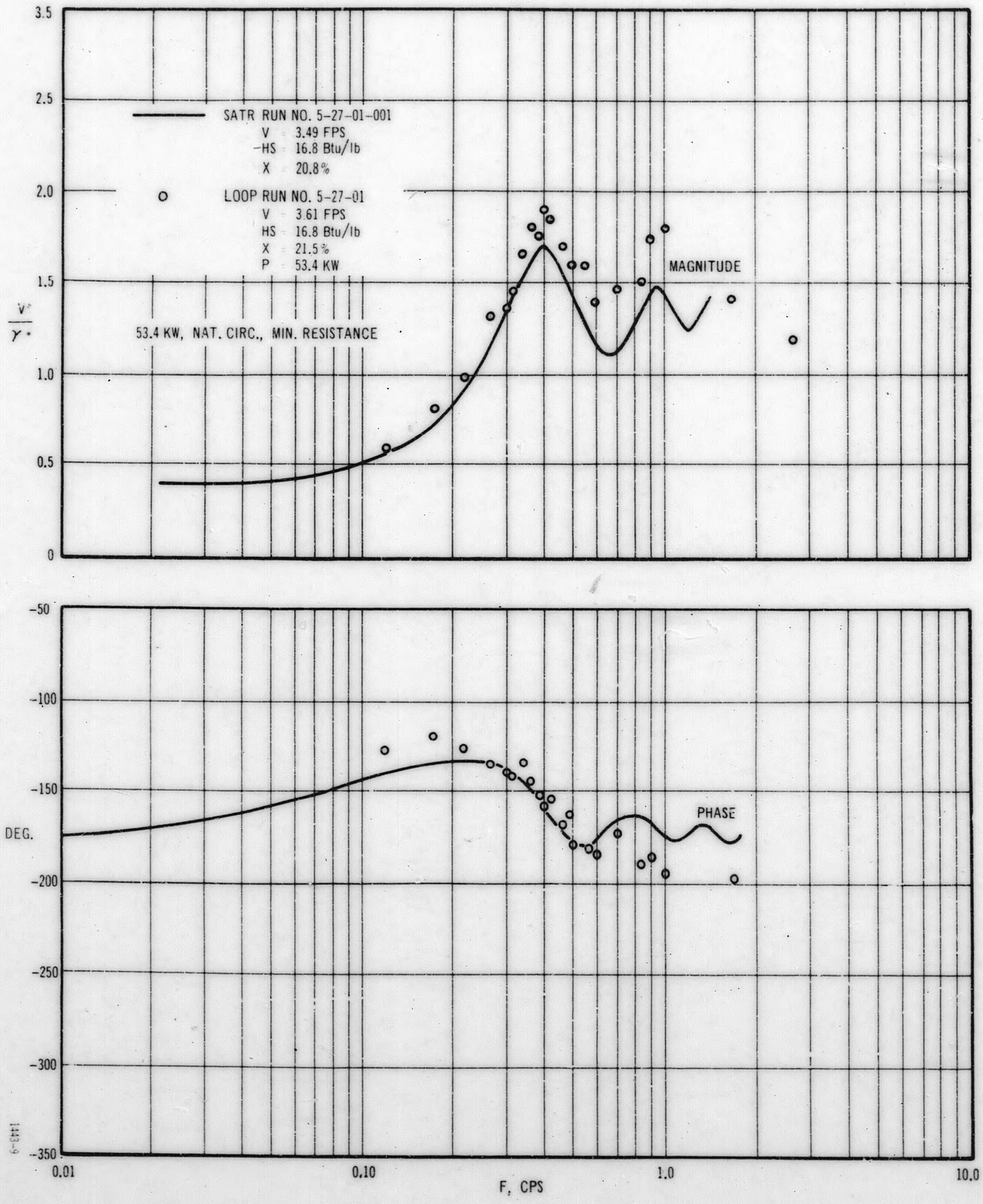

Figure 9. Velocity Response, Run 5-27-01

TASK B - HEAT TRANSFER AND FLUID DYNAMICS

The heat transfer task is being conducted to obtain design data on the critical heat flux, to gain understanding of the phenomena involved, and to raise the limit. The previous results of the program were summarized in the last quarterly report. The work has been terminated and the items reported here conclude this task.

A terminal topical report Critical Heat Flux for Multirod Geometry, GEAP-4358, by J. E. Hench, has been prepared. The 45 critical heat flux measurements were made with a four-rod geometry which is representative of a reactor multirod assembly. Comparison of the results to previous data* for a single rod indicates some improvement in critical heat flux with four rods.

Additional data obtained for critical heat flux with a single heated rod and a rough liner are given in Table VII. The data were obtained by Janssen and Kervinen, in March 1962, by methods previously described.* A plot of the data and sketch of the test geometry were shown in GEAP-4302,** and the data is also discussed in GEAP-4301 and GEAP-4215.** The tabulated data are given here to complete the reporting of this work. The rough liner results in an increase in critical heat flux, as discussed previously.

The rough liner had horizontal square rings (0.080-inch by 0.080-inch cross section) projecting into the flow stream. The spacing between rings was 0.50, 0.92, and 2.6 inches for the three geometries tested.

Run Number	Pressure	Geometry
1-37	600, 1000, 1400	Smooth Liner
38-54	1000	Rough Liner, S = 0.50 inch
55-73	1000	Rough Liner, S = 0.92 inch
74-88	1000	Rough Liner, S = 2.60 inch

The flow was vertically upward. The heated rod had a 0.375-inch OD, the channel had an 0.870-inch ID and the rings had a 0.710-inch ID. Heated length was 70 inches.

In the summary of the results of the heat transfer program presented in the last quarterly report, the tests made with a bowed heater rod in contact with the channel wall were neglected. The results reported in GEAP-4215, Eleventh Quarterly Progress Report, show that the critical heat flux is decreased by a factor of two or more from values obtained with normal clearances. Temperature measurements on the rod, when operated past the critical heat flux, were in the order of magnitude of 1000 F for heat fluxes of about 500,000 to 600,000 Btu/hr-ft^2.

*E. Janssen and J. A. Kervinen, GEAP-3899. (Previous reports of this program are listed on page v.)

**See page v for list of previous reports of this program.

TABLE VII

SINGLE ROD CRITICAL HEAT FLUX DATA
WITH SMOOTH AND ROUGH LINER

(See Text for Test Conditions)

Run No.	Pressure psia	W lb/sec	G × 0.000001 lb/hr ft^2	Sub-Cooling Btu/lb	q/A × 0.000001 Btu/hr ft^2	x Quality
B001	1004	0.530	0.569	16.3	0.649	0.2744
B002	995	0.506	0.543	72.5	0.695	0.2240
B003	1005	0.503	0.540	99.5	0.740	0.2067
B004	1000	0.511	0.549	145.0	0.864	0.1901
B005	1005	0.517	0.555	185.0	0.979	0.1782
B006	995	0.519	0.556	240.0	1.098	0.1485
B007	1000	1.054	1.131	25.0	0.792	0.1455
B008	1011	1.046	1.123	94.0	1.026	0.0953
B009	997	1.059	1.136	157.0	1.275	0.0528
B010	1008	1.051	1.127	219.5	1.516	0.0150
B011	1010	1.050	1.127	245.0	1.599	-0.0048
B012	1003	1.615	1.733	19.5	0.859	0.1001
B013	1003	1.587	1.703	53.5	1.002	0.0722
B014	1005	1.586	1.701	76.5	1.103	0.0524
B015	1005	1.582	1.698	101.7	1.222	0.0324
B016	1003	1.587	1.703	126.4	1.337	0.0114
B017	1000	1.590	1.706	152.5	1.458	-0.0105
B018	1000	1.054	1.131	25.0	0.778	0.1420
B019	1000	1.055	1.132	22.5	0.764	0.1425
B020	1000	1.057	1.134	99.5	1.053	0.0905
B021	1000	1.057	1.135	163.5	1.279	0.0442
B022	607	1.054	1.131	17.5	0.850	0.1512
B023	604	1.053	1.130	53.5	0.976	0.1282
B024	605	1.052	1.128	101.5	1.146	0.0979
B025	600	1.053	1.130	19.7	0.823	0.1430
B026	600	1.051	1.128	53.5	0.924	0.1177
B027	600	1.057	1.135	92.2	1.055	0.0906
B028	600	1.052	1.129	129.5	1.193	0.0694
B029	600	1.050	1.126	161.7	1.317	0.0516
B030	600	1.049	1.126	193.5	1.461	0.0378

(Continued)

TABLE VII (Continued)

Run No.	Pressure psia	W lb/sec	G × 0.000001 lb/hr ft^2	Sub-Cooling Btu/lb	q/A × 0.000001 Btu/hr ft^2	x Quality
B031	1410	1.053	1.129	31.5	0.673	0.1220
B032	1405	1.055	1.132	73.5	0.835	0.0911
B033	1400	1.062	1.139	98.1	0.907	0.0654
B034	1400	1.057	1.134	120.3	0.990	0.0497
B035	1405	0.529	0.567	48.5	0.549	0.2027
B036	1395	0.512	0.549	92.0	0.647	0.1891
B037	1405	0.514	0.551	148.0	0.811	0.1792
B038	1000	0.503	0.539	74.5	0.883	0.3151
B039	1000	0.508	0.545	115.0	0.909	0.2609
B040	1000	0.507	0.544	150.5	0.931	0.2177
B041	1000	0.508	0.545	176.2	0.979	0.2004
B042	1000	0.512	0.550	221.5	0.990	0.1319
B043	1000	0.514	0.551	254.7	1.067	0.1159
B044	1000	0.518	0.556	306.6	1.146	0.0688
B045	1000	1.053	1.130	25.0	0.974	0.1877
B046	1000	1.056	1.133	66.4	1.026	0.1355
B047	1000	1.054	1.131	102.0	1.076	0.0927
B048	1000	1.059	1.136	139.5	1.158	0.0527
B049	1001	1.055	1.132	182.5	1.267	0.0129
B050	1000	1.052	1.129	203.7	1.301	-0.0111
B051	1003	1.592	1.708	12.5	1.014	0.1367
B052	1000	1.585	1.700	73.5	1.172	0.0678
B053	1005	1.585	1.701	109.5	1.286	0.0299
B054	1005	1.572	1.687	138.5	1.372	0.0003
B055	1003	0.506	0.543	440.5	0.969	-0.2100
B056	1005	0.503	0.540	83.6	1.031	0.3727
B057	1005	0.506	0.542	126.5	1.055	0.3157
B058	1000	0.510	0.547	161.3	1.098	0.2784
B059	1003	0.516	0.553	203.7	1.146	0.2298
B060	1005	0.517	0.555	235.0	1.196	0.2041
B061	1011	0.517	0.555	275.9	1.222	0.1529
B062	1010	0.522	0.560	319.9	1.279	0.1072
B063	1005	1.047	1.124	25.0	1.005	0.1962
B064	1001	1.049	1.125	73.3	1.076	0.1382
B065	1001	1.057	1.134	120.5	1.169	0.0852

(Continued)

TABLE VII (Continued)

Run No.	Pressure psia	W lb/sec	G × 0.000001 lb/hr ft^2	Sub-Cooling Btu/lb	q/A × 0.000001 Btu/hr ft^2	x Quality
B066	1000	1.051	1.128	180.5	1.298	0.0242
B067	1005	0.925	0.992	210.0	1.399	0.0468
B068	1005	0.934	1.002	231.0	1.465	0.0281
B069	1005	1.593	1.709	12.5	1.074	0.1457
B070	1000	1.588	1.703	55.7	1.141	0.0900
B071	1000	1.590	1.706	93.0	1.241	0.0477
B072	1000	1.589	1.705	134.0	1.408	0.0105
B073	1000	1.589	1.705	161.0	1.527	-0.0127
B074	1005	0.489	0.524	54.5	0.902	0.3679
B075	1003	0.506	0.543	104.0	0.957	0.3023
B076	1003	0.506	0.543	108.5	0.990	0.3115
B077	1005	0.504	0.541	158.0	1.074	0.2776
B078	1001	0.507	0.544	207.0	1.110	0.2164
B079	1000	0.495	0.531	111.0	0.948	0.2977
B080	1005	0.511	0.549	227.0	1.098	0.1759
B081	1010	0.511	0.548	259.4	1.148	0.1500
B082	1010	1.058	1.135	38.0	1.041	0.1822
B083	1010	1.054	1.131	81.5	1.098	0.1293
B084	1005	1.054	1.131	166.7	1.260	0.0358
B085	997	1.055	1.132	199.5	1.322	-0.0005
B086	985	1.056	1.133	227.0	1.384	-0.0289
B087	1010	1.565	1.680	25.0	1.169	0.1443
B088	1010	1.569	1.683	64.0	1.246	0.0958

REFERENCES

1. Shober, F. R., "The Effect of Nuclear Radiation on Structural Metals," PEIC, Report No. 20, September, 1961.
2. "Examination of PWR Core 1 Blanket Fuel Rods for Microstructure Changes, Hydrogen Pickup, Burst Strength and Fission Gas Release at the End of the Second Seed Life," WAPD-TM-326, April, 1963.
3. High Power Density Development Project, Twelfth Quarterly Progress Report, GEAP-4219.
4. High Power Density Development Project, Thirteenth Quarterly Progress Report, GEAP-4309.
5. Sachs, G., and Espey, G., Trans. Am. Inst. Mining and Met. Engr., Inst. Metals Div. (1942), p. 348-360.
6. High Power Density Development Project, Eleventh Quarterly Progress Report, GEAP-4155, October-December, 1962.

ACKNOWLEDGMENT

The Fuel Cycle Program is sponsored by the AEC and is conducted by the General Electric Company with the following individuals contributing to the program during the quarter:

Project Engineer	C. L. Howard
Project Consultant	S. Levy
Fuel Development	T. J. Pashos
	H. E. Williamson
	C. J. Baroch
	J. P. Hoffman
	F. H. Megerth
	S. Y. Ogawa
	J. A. Whittington
Stability	W. H. Cook
Heat Transfer and Fluid Dynamics	E. Janssen
	J. E. Hench
VBWR Core Analysis	J. O. Arterburn
	R. A. Becker
	T. Tillinghast
VBWR Programming	H. D. Ongman
VBWR Operation	J. B. Violette
Test Program Engineering	E. L. Burley
	R. H. Silletto
	VBWR Staff
Vallecitos Radioactive Material Laboratory	R. F. Boyle

END